Adipocyte-derived exosomal miR-30c-5p promotes ovarian angiogenesis in polycystic ovary syndrome via the SOCS3/STAT3/VEGFA pathway

Jian Hu[1,2,*,#], Fangyou Lin[3,*,#], Yuchen Yin[1,2], Yunjie Shang[1,2], Zhuoni Xiao[1,2], Wangming Xu[1,2]

[1]Reproductive Medical Center, Renmin Hospital of Wuhan University, Wuhan 430060, China
[2]Hubei Clinic Research Center for Assisted Reproductive Technology and Embryonic Development, Wuhan 430060, China
[3]Department of Urology, Renmin Hospital of Wuhan University, Wuhan 430060, China
*Equal contribution
#Co-first author

Correspondence to: Zhuoni Xiao, Wangming Xu; **email:** RM001111@whu.edu.cn, 15927618487@163.com

ABSTRACT

Polycystic ovary syndrome (PCOS) is a systemic endocrine disease affecting the reproductive health of women. Ovarian angiogenesis in PCOS patients exhibits abnormal, manifested as increased ovarian stromal vascularization and upregulated proangiogenic factors such as vascular endothelial growth factor (VEGF). However, the specific mechanisms underlying these changes in PCOS remain unknown. In this study, we induced the adipogenic differentiation of preadipocyte 3T3-L1 cells and found that adipocyte-derived exosomes promoted proliferation, migration, tube formation and VEGFA expression in human ovarian microvascular endothelial cells (HOMECs) by delivering miR-30c-5p. Mechanistically, dual luciferase reporter assay demonstrated that miR-30c-5p directly targeted the 3'- untranslated region (UTR) of suppressor of cytokine signaling 3 (SOCS3) mRNA. In addition, adipocyte-derived exosomal miR-30c-5p activated signal transducer and activator of transcription 3 (STAT3)/VEGFA pathway in HOMECs via targeting SOCS3. *In vivo* experiments indicated that tail vein injection of adipocyte-derived exosomes exacerbated endocrine and metabolic disorders and ovarian angiogenesis in mice with PCOS via delivery of miR-30c-5p. Taken together, the study revealed that adipocyte-derived exosomal miR-30c-5p promotes ovarian angiogenesis via the SOCS3/STAT3/VEGFA pathway, thereby participating in the pathogenesis of PCOS.

INTRODUCTION

Polycystic ovary syndrome (PCOS) is a common endocrine disease among women of reproductive age, which is reported in approximately 5–10% women worldwide [1]. The etiology of PCOS remains unclear but may be associated with genetic and environmental factors. According to the Rotterdam consensus, women who present with at least two of the following symptoms should be diagnosed as having PCOS: clinical or biochemical hyperandrogenism, oligo-ovulation or anovulation and the presence of polycystic ovaries on ultrasonography [2]. However, the diagnosis and treatment of PCOS remain a great challenge owing to the great heterogeneity of this systemic disease. Therefore, understanding the pathogenesis of PCOS is important for developing new diagnostic and treatment methods.

Angiogenesis refers to the formation of new blood vessels from existing vessels, which dominantly entails the activation, proliferation, and migration of endothelial cells (ECs) and is counterbalanced by proangiogenic and antiangiogenic factors [3]. In

sexually mature female mammals, the vasculature of reproductive system presents periodical regeneration and degeneration. The periodical formation and regression of ovarian blood vessels provide necessary nutrients and hormones for follicular growth, ovulation, luteum formation and secretion of ovarian hormones [4]. Interestingly, ovarian angiogenesis is abnormal in PCOS patients, manifested as increased ovarian stromal vascularization [5, 6]. In addition, the expression of angiogenic factors such as VEGF in PCOS women is altered [7]. VEGF is one of the most significant angiogenic factors in PCOS, which has been reported to be upregulated in the ovaries, serum, and follicular fluid of patients with PCOS [8–10]. Besides, serum VEGF levels in obese PCOS patients are significantly higher than in non-obese PCOS patients [11]. Moreover, a positive correlation is found between the levels of serum VEGF and ovarian vascularization [12]. Nevertheless, the specific mechanisms leading to the increase in VEGF levels and ovarian stromal vascularization in PCOS patients remain unclear.

Approximately 50% patients with PCOS are obese [13]. Obesity, which is characterized by the deposition of adipose tissue (AT), aggravates endocrine and metabolic disorder in PCOS patients. As the major constituent of AT, adipocytes secret adipokines (such as leptin, adiponectin and resistin) that are involved in the development of PCOS-related weight gain, insulin resistance, inflammation, and granulosa apoptosis, which denotes obesity modifies PCOS manifestations by adipocytes [14]. Exosomes are extracellular vesicles (EVs) with a diameter of 30–200 nm, which are responsible for cell–cell communication. Donor cells can regulate the biological function of recipient cells by delivering the contents of exosomes, such as proteins, lipids, mRNAs and noncoding RNAs (ncRNAs) [15]. As energy-saving and endocrine cells, adipocytes exert great metabolic regulatory effects [16]. Notably, studies have indicated that adipocyte-derived exosomes participate in the regulation of glucose metabolism, lipid synthesis and endothelial injury as a new type of adipokines, providing a new explanation for the pathogenesis of obesity-related diseases [17–19]. However, to the best of our knowledge, no study has explored the role of adipocyte-derived exosomes in the pathogenesis of PCOS.

MicroRNAs (miRNAs) are short endogenous ncRNAs that have been widely studied as the functional contents of exosomes owing to their strong regulatory effects on gene expression. AT is an important source of exosomal miRNAs in the circulatory system [20]. As a member of the miR-30 family, miR-30c-5p is usually recognized as a regulator of adipogenesis, pathological cardiac remodeling, tumour invasion and angiogenesis [21, 22].

The expression of miR-30c-5p was upregulated during the adipogenesis of human multipotent adipose-derived stem cells. Besides, miR-30c-5p overexpression boosted adipocyte marker gene expression and triglyceride accumulation [23]. A previous study found miR-30c-5p promoted tube formation in human umbilical vein endothelial cells (HUVECs) *in vitro*, and downregulation of miR-30c-5p in zebrafish significantly inhibited angiogenesis *in vivo* [24]. Moreover, the serum levels of miR-30c are higher in PCOS patients [25]. Taken together, we hypothesized that adipocyte-derived exosomes might be involved in the pathogenesis of PCOS by delivering miR-30c-5p to promote ovarian angiogenesis and verified this hypothesis by performing experiments described below.

RESULTS

Adipocyte-derived exosomes were internalized by HOMECs

Adipogenic differentiation of 3T3-L1 cells was induced to imitate mature adipocytes *in vivo*. Differentiated 3T3-L1 cells exhibited typical adipocyte phenotypes as indicated by oil red O staining (Figure 1A). Exosomes from differentiated adipocytes were isolated via ultracentrifugation and identified via transmission electron microscopy (TEM), nanoparticle tracking analysis (NTA) and western blotting. TEM revealed the presence of vesicles with a bi-layer membrane structure ranging from 30 to 200 nm (Figure 1B). The average diameter of the vesicles was 136.3 nm detected by NTA (Figure 1C). Western blotting revealed the expression of exosome markers, namely, CD9 and CD63, in isolated vesicles. Fatty acid binding protein 4 (FABP4) is a specific marker of adipocyte-derived exosomes [26], which was detected in differentiated 3T3-L1 cells and vesicles (Figure 1D). Above results indicated we successfully isolated adipocyte-derived exosomes. To assess whether HOMCEs can internalize adipocyte-derived exosomes, HOMECs were incubated with PKH-26 labelled exosomes, while PBS was added as the control (CON). After 6 h, PKH26-labelled exosomes were observed in HOMECs (Figure 1E). Altogether, these results indicated that adipocyte-derived exosomes were internalized by HOMECs.

Adipocyte-derived exosomes promoted proliferation, migration, and tube formation in HOMECs

To assess the effects of adipocyte-derived exosomes on the biological function of HOMECs, exosomes at different concentrations were added to HOMECs according to the exosome concentrations reported in previous studies [27, 28]. The results of cell counting kit-8 (CCK-8) assay demonstrated that the

proliferation rate of HOMECs treated with exosomes was significantly higher than that in the control group (Figure 2A). In addition, the protein expression of Ki67 and proliferating cell nuclear antigen (PCNA) was upregulated in HOMECs treated with exosomes, indicating that adipocyte-derived exosomes strengthened HOMEC proliferation (Figure 2B).

Compared with PBS treatment, exosome treatment promoted the migration of HOMECs as indicated by an increased number of migrated cells, upregulation of Vimentin and downregulation of E-cadherin (Figure 2C, 2D). Furthermore, tube formation assay indicated that exosomes enhanced the capillary-like structure formation capacity of HOMECs as indicated by the
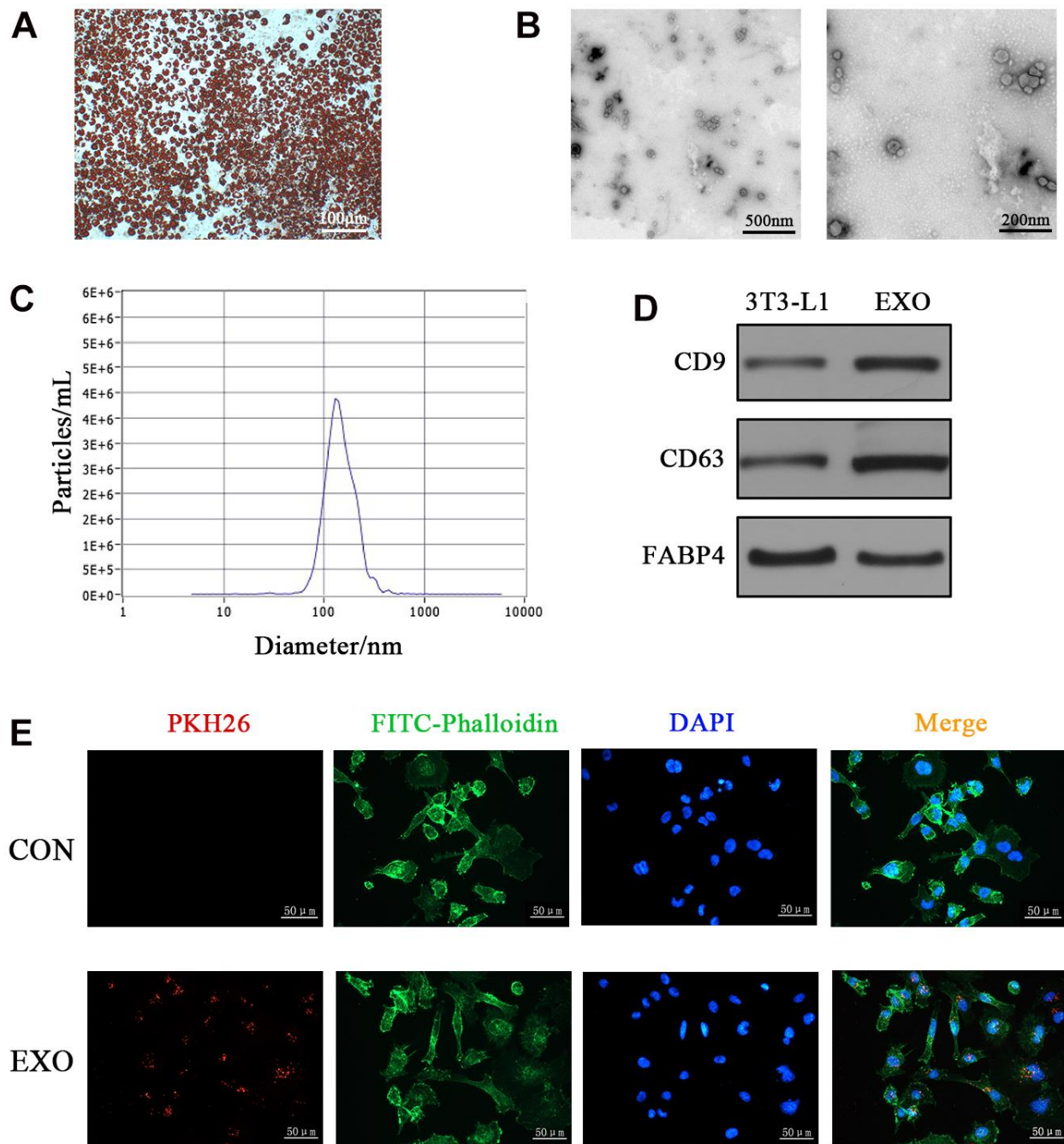

Figure 1. Characterization of adipocyte-derived exosomes. (**A**) Oil red O staining of differentiated 3T3-L1 cells. (**B**) TEM analyses of exosomes secreted by adipocytes. (**C**) NTA of exosomes. (**D**) Western blotting analyses of exosomal markers (CD9, CD63 and FABP4) in 3T3-L1 cells and adipocyte-derived exosomes. (**E**) Fluorescence images of HOMECs incubated with PKH26-labelled exosomes (red). The cytoskeleton was stained with phalloidin-FITC (green), and nuclei were stained with DAPI (blue).

increased total tube length and number of branches (Figure 2E). Western blotting verified that exosomes enhanced the expression of VEGFA in HOMECs (Figure 2F). Altogether, these results showed that adipocyte-derived exosomes promoted proliferation, migration, and tube formation in HOMECs. Because 20 µg/mL exosomes exerted greater effects on the biological function and protein expression in HOMECs than 10 µg/mL exosomes, the exosome concentration of 20 µg/mL was selected for subsequent cell experiments.

miR-30c-5p was delivered by adipocyte-derived exosomes and promoted proliferation, migration, and tube formation in HOMECs

A coculture system was used to verify that adipocyte-derived exosomes delivered miR-30c-5p to HOMECs (Figure 3A). The levels of miR-30c-5p were increased in HOMECs co-cultured with differentiated 3T3-L1 cells but were decreased after adipocytes were treated with the exosome inhibitor GW4869 (Figure 3B). These results indicated that miR-30c-5p was delivered to HOMECs by exosomes. Furthermore, miR-30c-5p mimics/inhibitors/negative controls (NCs) were

transfected into HOMECs to investigate the effects of miR-30c-5p on the biological function of HOMECs. The miR-30c-5p levels in HOMECs were significantly increased after transfection of miR-30c-5p mimics while they were decreased after transfection of miR-30c-5p inhibitors (Figure 3C). Subsequently, the role of miR-30c-5p in the proliferation, migration, and tube formation of HOMECs was examined. The results of CCK-8 assay demonstrated that the miR-30c-5p overexpression enhanced the proliferation rate of HOMECs whereas miR-30c-5p inhibition suppressed HOMEC proliferation (Figure 3D). The number of migrated HOMECs was increased after the transfection of miR-30c-5p mimics but decreased after the transfection of miR-30c-5p inhibitors (Figure 3E, 3F). In addition, tube formation assays suggested miR-30c-5p enhanced capillary-like structure formation capacity of HOMECs (Figure 3G, 3H).

miR-30c-5p activated the STAT3/VEGFA pathway by targeting SOCS3

To determine the mechanism of miR-30c-5p regulating biological function of HOMECs, the target genes of miR-30c-5p were predicted via bioinformatic analysis.
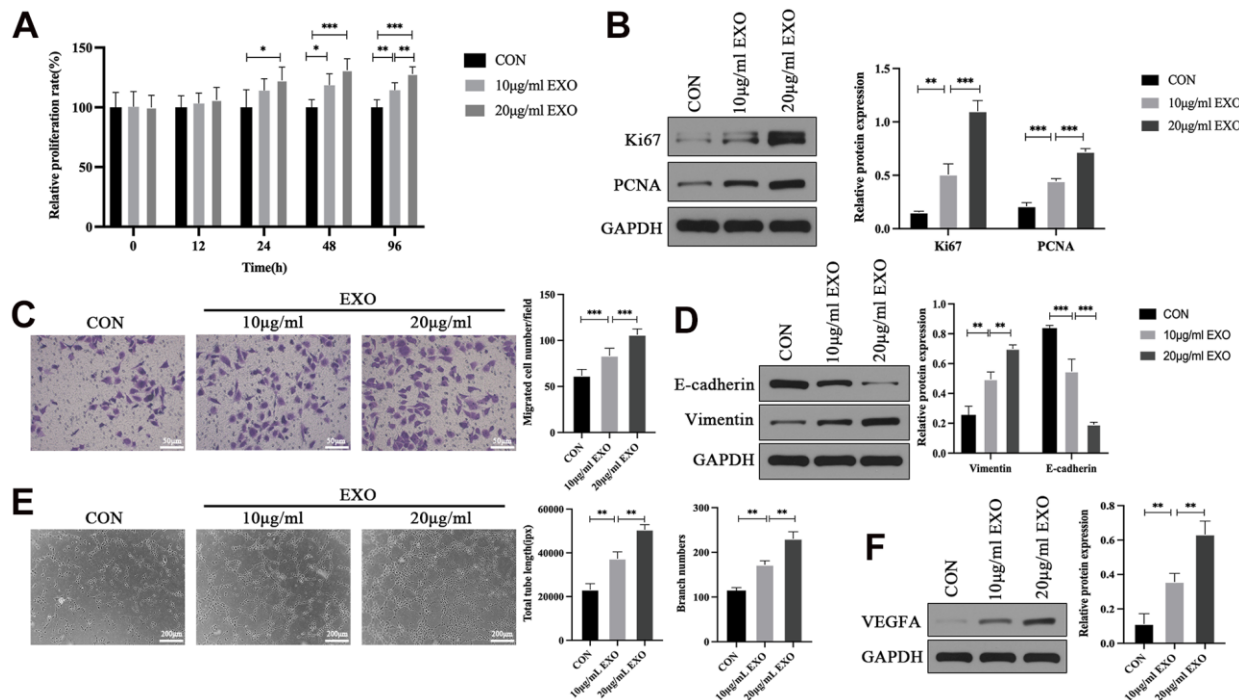

Figure 2. Adipocyte-derived exosomes promote proliferation, migration, and tube formation in HOMECs. (**A**) Detection of the effect of adipocyte-derived exosomes on the cell proliferation by the CCK-8 assay. (**B**) Western blotting analyses of Ki67 and PCNA expression in HOMECs. (**C**) Detection of the effect of adipocyte-derived exosomes on the cell migration by the transwell assay. (**D**) Western blotting analyses of E-cadherin and Vimentin expression in HOMECs. (**E**) Detection of the effect of adipocyte-derived exosomes on the cell tube formation by the tube formation assay. (**F**) Western blotting analyses of VEGFA expression in HOMECs. Data are presented as mean ± SD for three independent experiments. *P<0.05, **P<0.01, ***P<0.001.

The results indicated that SOCS3 was one of the 12 target genes of miR-30c-5p jointly predicted by TargetScan, miRDB and Starbase (Figure 4A, 4B). TargetScan predicted that the 3'-UTR of the SOCS3 mRNA was the conserved binding site of miR-30c-5p (Figure 4C). Furthermore, the results of dual luciferase reporter assay showed that the transfection of miR-30c-5p mimics reduced the luciferase activity in HOMECs transfected with *pmirGLO-SOCS3-WT* instead of *pmirGLO-SOCS3-MUT* (Figure 4D). These results
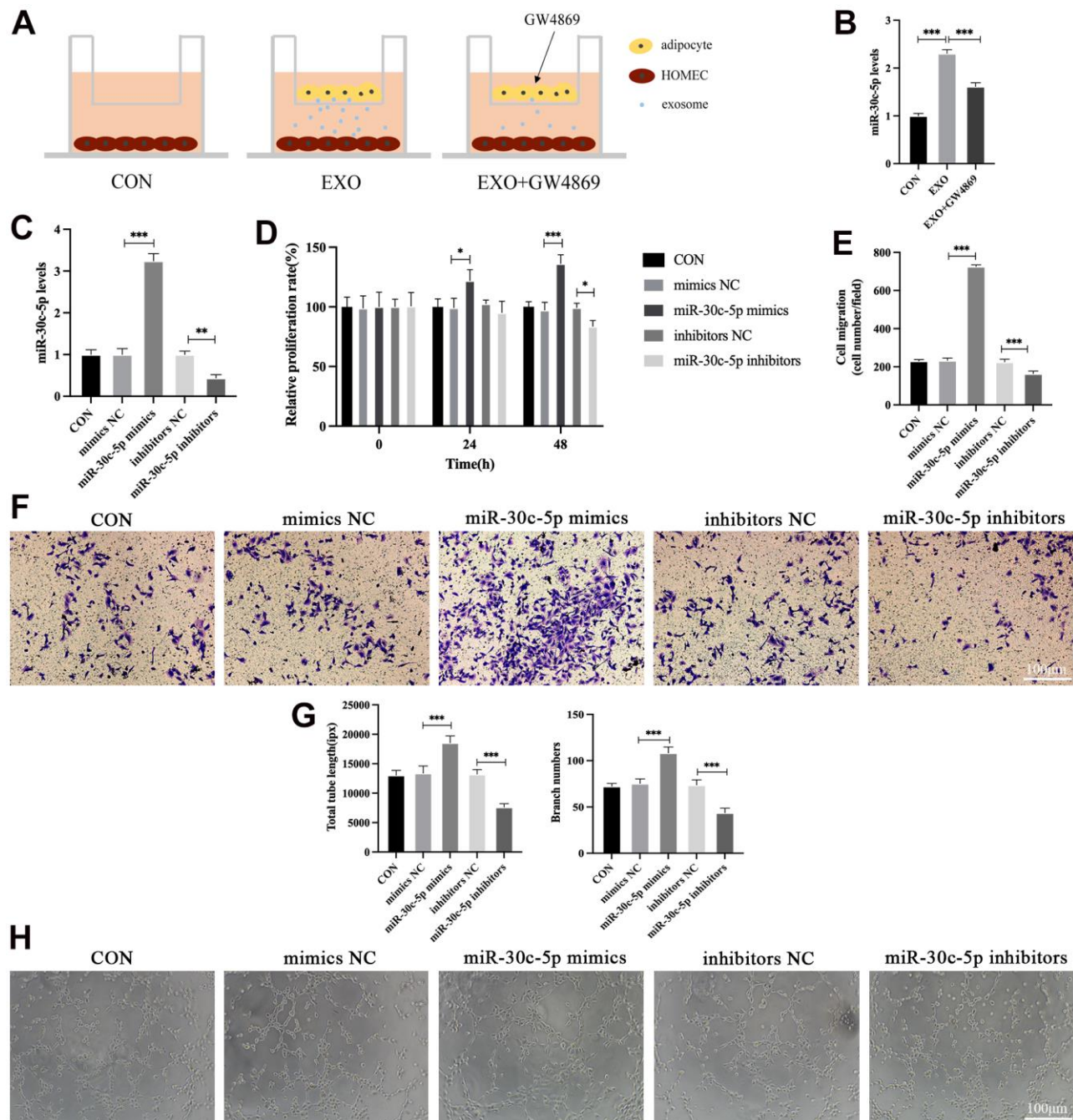

Figure 3. miR-30c-5p is delivered by adipocyte-derived exosomes and promotes proliferation, migration, and tube formation in HOMECs. (**A**) Coculture of HOMECs and adipocytes treated with or without GW4869. (**B**) qRT-PCR detection of miR-30c-5p levels in HOMECs in the coculture system. (**C**) qRT-PCR detection of miR-30c-5p levels after cell transfection. (**D**) Detection of the effect of miR-30c-5p on the cell proliferation by the CCK-8 assay. (**E**, **F**) Detection of the effect of miR-30c-5p on the cell migration by the transwell assay. (**G**, **H**) Detection of the effect of miR-30c-5p on the cell tube formation capacity by the tube formation assay. Data are presented as mean ± SD for three independent experiments. *P<0.05, **P<0.01, ***P<0.001.

indicated that miR-30c-5p inhibited the transcription of SOCS3 by directly binding to the 3'-UTR of SOCS3 mRNA.

SOCS3 can indirectly inhibit the transcription of VEGFA by inhibiting STAT3 [29, 30]. Therefore, the effects of miR-30c-5p on the SOCS3/STAT3/VEGFA pathway were further investigated. Western blotting showed that overexpression of miR-30c-5p suppressed the expression of SOCS3 and promoted the expression of p-STAT3 and VEGFA, whereas miR-30c-5p inhibition significantly upregulated the expression of SOCS3 and inhibited the expression of p-STAT3 and VEGFA (Figure 5A). Furthermore, HOMECs were co-transfected with miR-30c-5p mimics and SOCS3 plasmid to investigate the effects of the miR-30c-5p/SOCS3 axis on the STAT3/VEGFA pathway. The results showed transfection of only miR-30c-5p mimics led to

downregulation of SOCS3 and upregulation of p-STAT3 and VEGFA, while this effect was reversed after co-transfection with the SOCS3 plasmid (Figure 5B). Therefore, these results suggest that miR-30c-5p activates the STAT3/VEGFA pathway by targeting SOCS3.

Adipocyte-derived exosomal miR-30c-5p promoted proliferation, migration, and tube formation in HOMECs and activating the SOCS3/STAT3/VEGFA pathway

To verify whether miR-30c-5p mediates the effects of adipocyte-derived exosomes on the biological function of HOMECs, HOMECs were co-treated with miR-30c-5p inhibitors and adipocyte-derived exosomes. qRT-PCR showed that exosome treatment enhanced the levels of miR-30c-5p in HOMECs, whereas this effect was mitigated after co-treatment with miR-30c-5p
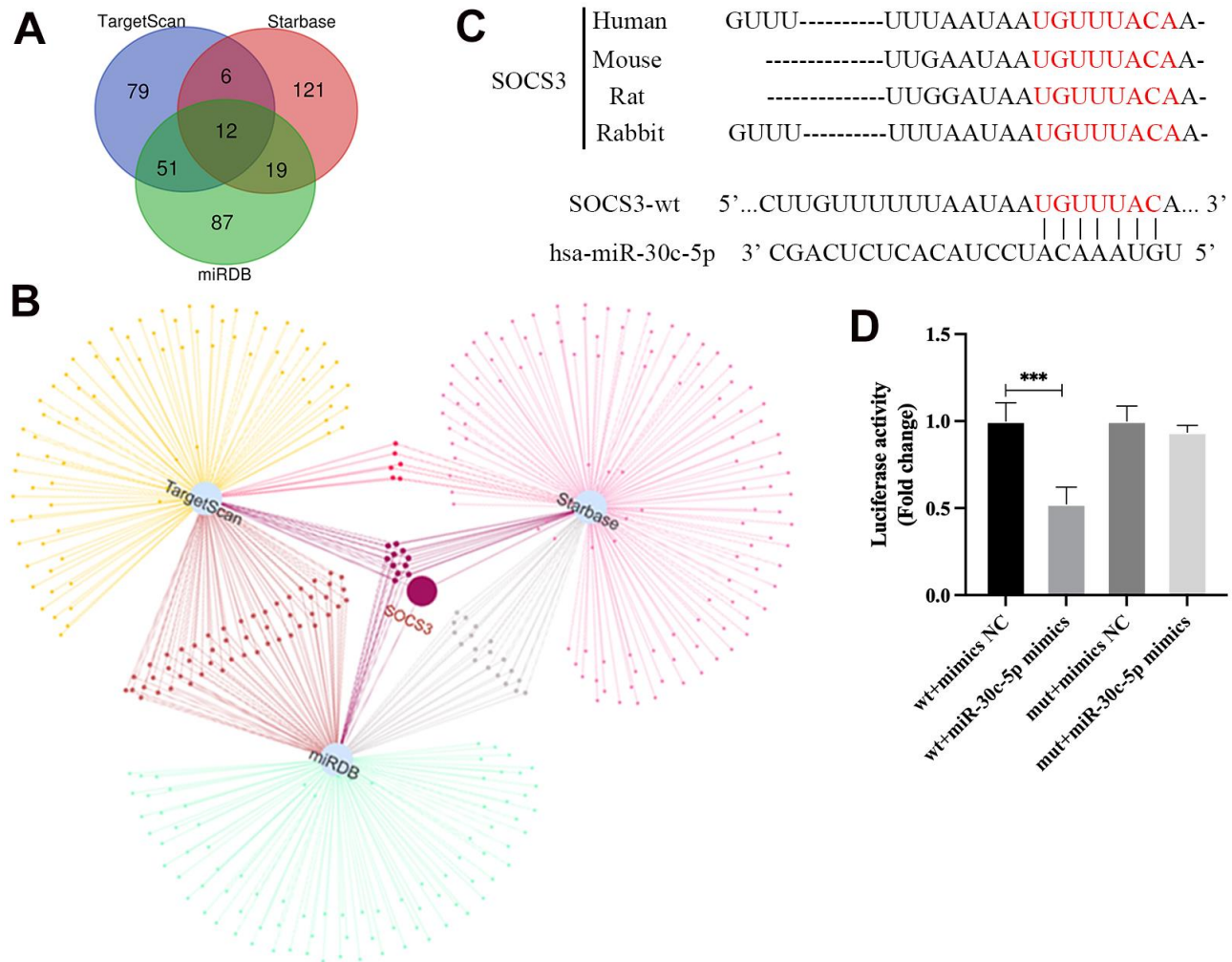

Figure 4. SOCS3 is a target gene of miR-30c-5p. (**A**, **B**) Bioinformatic analyses of target genes of miR-30c-5p. (**C**) Prediction of the binding site of miR-30c-5p in the 3'-UTR of SOCS3 mRNA by TargetScan. (**D**) Confirmation of the targeting relationship between miR-30c-5p and SOCS3 by the dual luciferase reporter assay. Data are presented as mean ± SD for three independent experiments. ***$P<0.001$.

inhibitors (Figure 6A). Furthermore, the effects of exosomal miR-30c-5p on the proliferation of HOMECs were examined, and the results revealed that miR-30c-5p inhibitors reversed the stimulative effects of exosomes on the proliferation of HOMECs (Figure 6B). In addition, wound healing assay indicated that miR-30c-5p inhibitors reversed the stimulative effects of exosomes on the migration of HOMECs (Figure 6C).Moreover, tube formation ability of HOMECs simultaneously treated with exosomes and miR-30c-5p inhibitors was weaker than that of HOMECs treated with only exosomes (Figure 6D). Western blotting revealed that exosomes stimulated p-STAT3 and VEGFA expression and suppressed SOCS3 expression

in HOMECs, while these effects were alleviated after miR-30c-5p inhibition (Figure 6E).

Adipocyte-derived exosomal miR-30c-5p exacerbated endocrine and metabolic disorders in mice with PCOS

To verify the abovementioned findings *in vivo*, dehydroepiandrosterone (DHEA) was used to induce PCOS in mice, and mice with PCOS were treated with adipocyte-derived exosomes and miR-30c-5p antagomir via tail vein injection (Figure 7A). DHEA-treated mice exhibited a disordered estrous cycle and weight gain, with the formation of cystic follicles (CFs) and deterioration of corpus luteum (CL) in the ovaries,
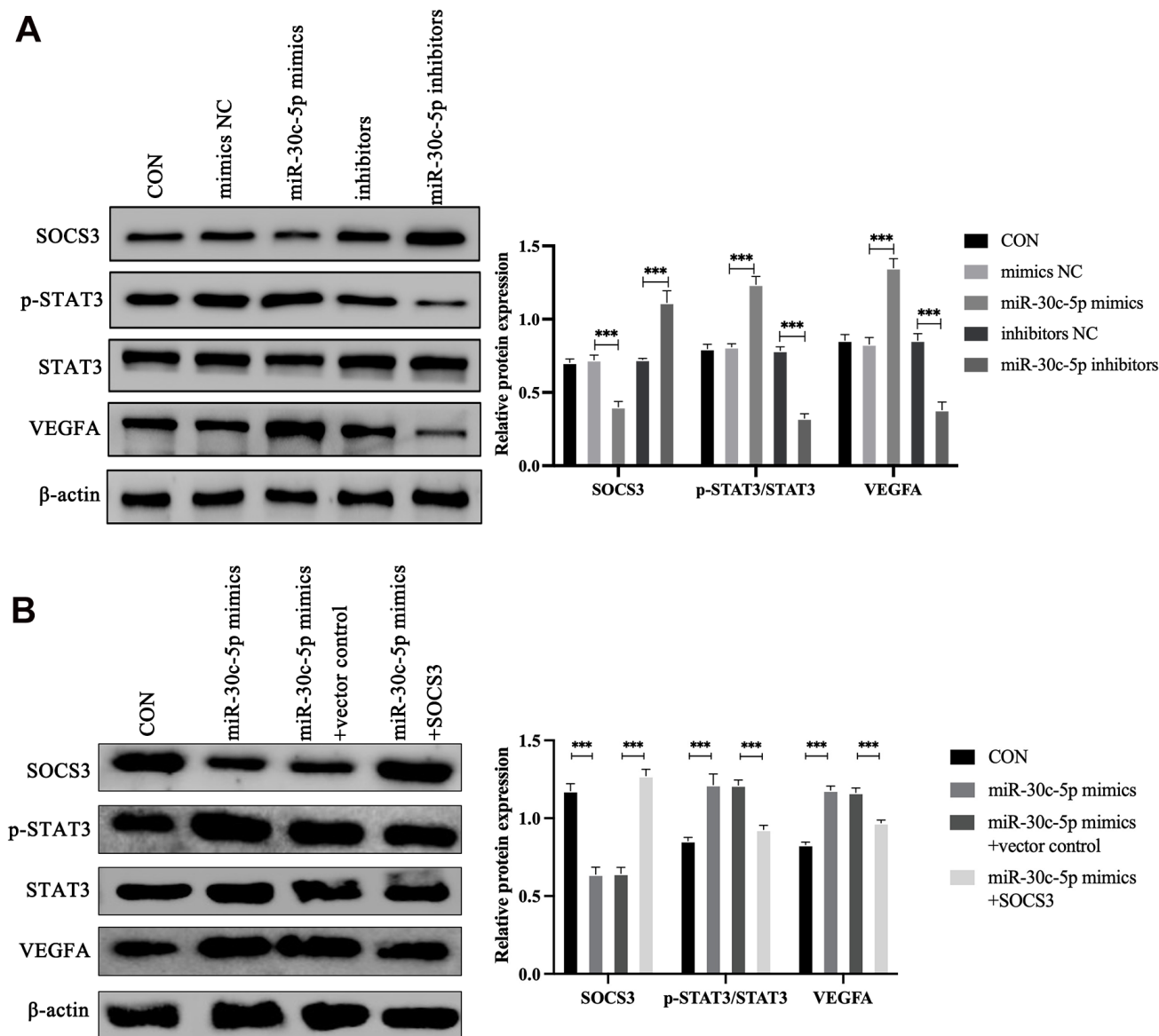

Figure 5. miR-30c-5p regulates the expression of the SOCS3/STAT3/VEGFA pathway. (**A**) Western blotting analyses of the effect of miR-30c-5p on SOCS3/STAT3/VEGFA pathway expression in HOMECs. (**B**) Western blotting analyses of the effect of SOCS3 on STAT3/VEGFA pathway expression in HOMECs. Data are presented as mean ± SD for three independent experiments. ***$P<0.001$.
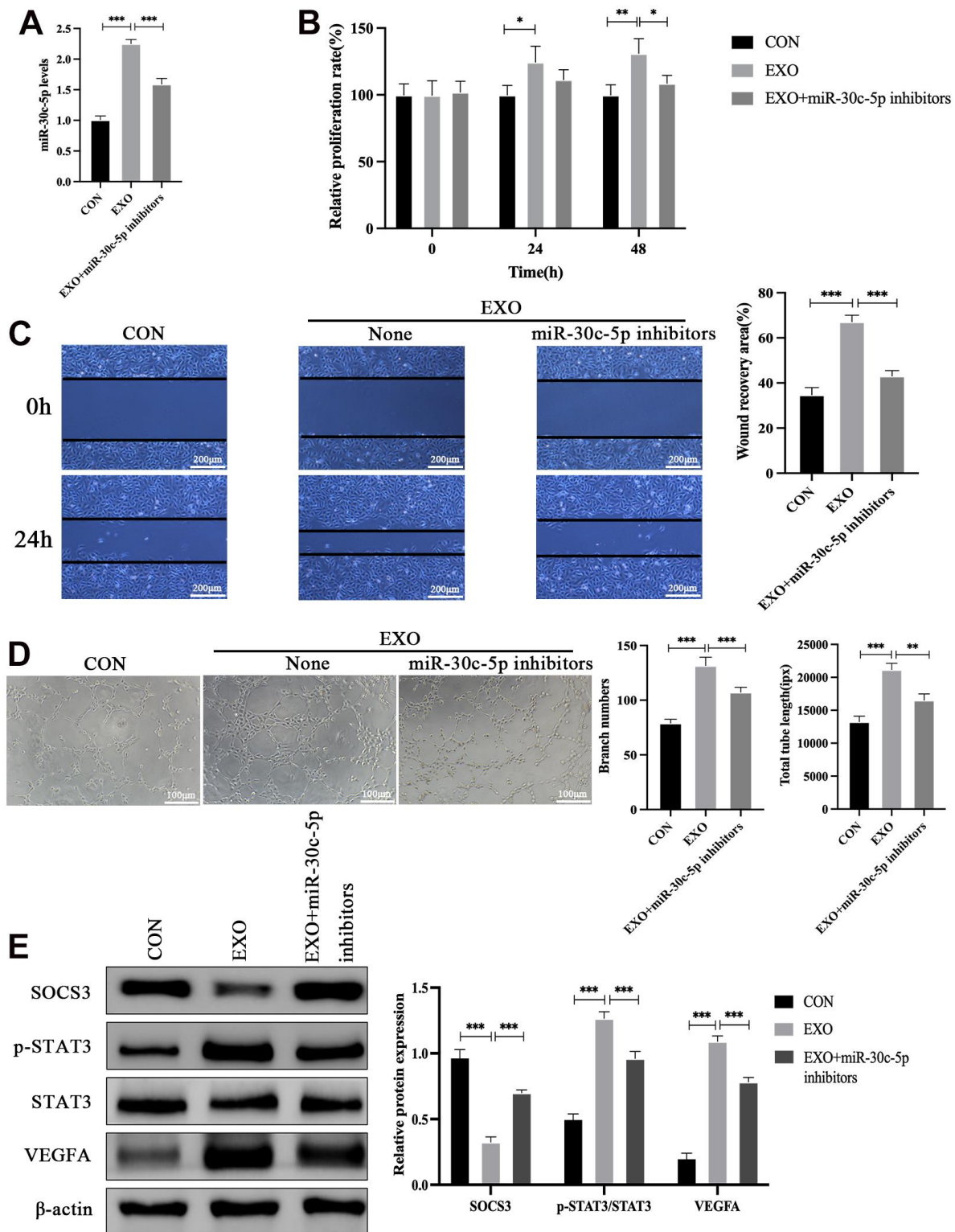
Figure 6. miR-30c-5p mediates the effects of adipocyte-derived exosomes on the biological function of HOMECs and the SOCS3/STAT3/VEGFA pathway. (**A**) qRT-PCR detection of the effect of exosomes combined with or without miR-30c-5p inhibitors on miR-30c-5p levels in HOMECs. (**B**) Detection of the effect of exosomal miR-30c-5p on the cell proliferation by the CCK-8 assay. (**C**) Detection of the effect of exosomal miR-30c-5p on the cell migration by the wound healing assay. (**D**) Detection of the effect of exosomal miR-30c-5p on the cell tube formation capacity by the tube formation assay. (**E**) Western blotting analyses of the effect of exosomal miR-30c-5p on SOCS3/STAT3/VEGFA pathway expression in HOMECs. Data are presented as mean ± SD for three independent experiments. *P<0.05, ** P<0.01, ***P<0.001.
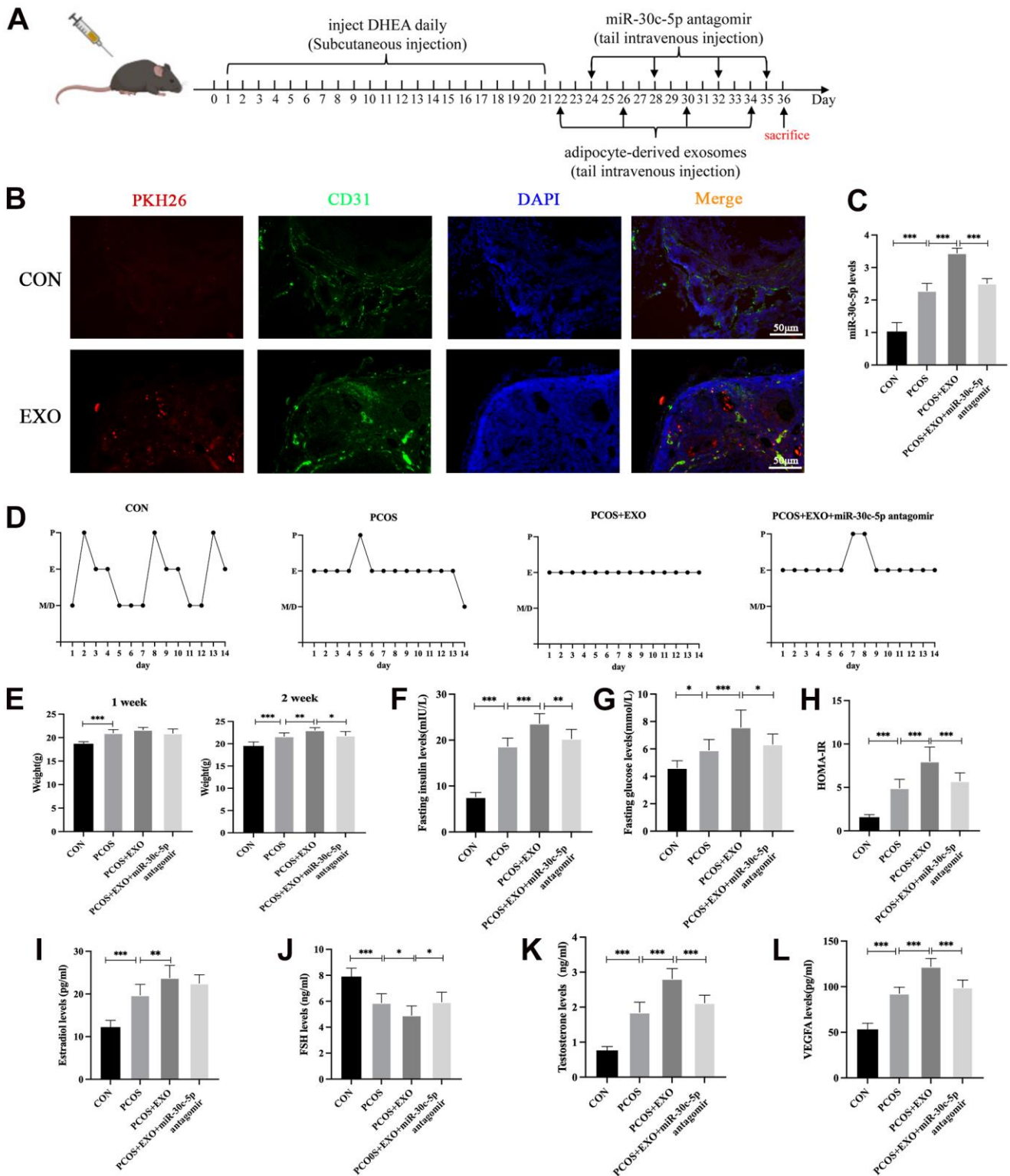
Figure 7. Adipocyte-derived exosomal miR-30c-5p exacerbates endocrine and metabolic disorders in mice with PCOS. (**A**) Procedure of animal experiments. (**B**) Visualization of uptake of exosomes by the ovaries *in vivo*. (**C**) qRT-PCR detection of miR-30c-5p levels in the ovaries of mice in the indicated groups. (**D**) Estrous cycle analyses of mice in each group via vaginal smears. (**E**) Weight change in the indicated groups after administration of exosomes and miR-30c-5p antagomir for 1 and 2 weeks. (**F**) Fasting insulin levels in the indicated groups. (**G**) Fasting glucose levels in the indicated groups. (**H**) HOMA-IR index in the indicated groups. HOMA-IR = fasting insulin × fasting glucose/22.5. (**I–L**) ELISA detection of serum E_2, FSH, T and VEGFA levels in the indicated groups. Proestrus (P), estrus (E), metestrus (M) and diestrus (D). Data are presented as mean ± SD for three independent experiments. *$P<0.05$, ** $P<0.01$, ***$P<0.001$.

indicating the establishment of PCOS models (Supplementary Figure 1A–1C). Immunofluorescence (IF) analyses of the ovaries showed that exosomes in blood circulation were taken up by the ovaries (Figure 7B). miR-30c-5p levels of the ovaries were increased in mice with PCOS. In the exosome-treated groups, exosome treatment alone increased miR-30c-5p levels in the ovaries of PCOS mice, but this effect was mitigated after co-treatment with miR-30c-5p antagomir. (Figure 7C). Notably, exosome treatment combined with or without miR-30c-5p antagomir had no significant effect on the estrous cycle of PCOS mice (Figure 7D). Additionally, PCOS mice gained weight after exosome treatment for 2 weeks, while miR-30c-5p antagomir alleviated this effect (Figure 7E). Furthermore, the glucometabolic state of mice in different groups was evaluated. The results demonstrated that miR-30c-5p antagomir mitigated the effects of exosomes on aggravating insulin resistance in PCOS mice (Figure 7F–7H). Exosome treatment downregulated serum follicle-stimulating hormone (FSH) levels and upregulated serum estradiol (E_2), testosterone (T) and VEGFA levels in PCOS mice. However, miR-30c-5p antagomir attenuated these changes (Figure 7I–7L). These results indicate that adipocyte-derived exosomes exacerbate endocrine and metabolic disorders in PCOS via miR-30c-5p.

Adipocyte-derived exosomal miR-30c-5p mediated ovarian angiogenesis through the SOCS3/STAT3/VEGFA pathway

In *in vivo* experiments, exosome treatment increased the number of CFs and deteriorated CL in the ovaries of PCOS mice. Nevertheless, miR-30c-5p antagomir attenuated these changes (Figure 8A). Ovarian angiogenesis was determined via immunohistochemical (IHC) analyses, which suggested that adipocyte-derived exosomes facilitated ovarian angiogenesis as shown by the downregulation of SOCS3 and upregulation of CD31 and VEGFA expression in ovaries. In addition, compared with PCOS mice treated with only exosomes, ovarian angiogenesis was inhibited in mice simultaneously treated with exosomes and miR-30c-5p antagomir (Figure 8B). Western blotting indicated adipocyte-derived exosomes suppressed SOCS3 expression and upregulated p-STAT3 and VEGFA expression in the ovaries of PCOS mice. Moreover, miR-30c-5p antagomir partially reversed the effects of adipocyte-derived exosomes on the expression of the SOCS3/STAT3/VEGFA pathway in ovaries (Figure 8C).

DISCUSSION

Balanced ovarian angiogenesis is essential for normal ovarian function. Therefore, elucidating the pathogenesis of abnormal ovarian angiogenesis and VEGF expression in PCOS is of great significance. In the present study, we found adipocyte-derived exosomes not only promoted proliferation, migration, and tube formation in HOMECs but also enhanced VEGFA expression. In addition, miR-30c-5p mediated the effects of adipocyte-derived exosomes on regulating the biological function of HOMECs and activating the STAT3/VEGFA pathway by targeting SOCS3. Furthermore, adipocyte-derived exosomal miR-30c-5p also participated in the development of endocrine and metabolic disorders, ovarian angiogenesis and VEGFA upregulation in PCOS mice. Overall, this study provides novel insights into the aetiology and pathology of PCOS.

An extracellular vesicle axis has been reported between ECs and adipocytes. ECs transfer caveolin 1-containing EVs to neighbouring adipocytes, whereas adipocytes reciprocate by releasing EVs to ECs. This reciprocal communication indicates that adipocytes and ECs can mutually regulate their functions through EVs [31]. Adipocyte-derived exosomal small nucleolar RNA host gene 9 (SNHG9) alleviated inflammation and apoptosis in ECs by targeting TNF receptor-associated death domain (TRADD), thus participating in the development of obesity-related endothelial cell dysfunction [19]. Moreover, insulin-resistant adipocyte-derived exosomes enhanced capillary-like structure formation capacity in HUVECs and promote vasa vasorum angiogenesis *in vivo* via Shh [27]. Our study showed that adipocyte-derived exosomes promoted proliferation, migration, and tube formation in HOMECs. VEGFA (also referred to as VEGF) is the main promoter of angiogenesis, which promotes EC proliferation and migration and vascular permeability by binding to its receptor [32]. In this study, adipocyte-derived exosomes enhanced VEGFA expression both in HOMECs and ovaries. Therefore, we suggest adipocyte-derived exosomes are involved in ovarian angiogenesis in PCOS.

Insulin resistance and obesity are common complications of PCOS. Previous studies have reported that adipocyte-derived exosomes can induce insulin resistance and energy metabolism dysfunction by regulating the function and phenotypic transformation of skeletal muscle, macrophages and pro-opiomelanocortin neurons [17, 33, 34]. In this study, adipocyte-derived exosomes exacerbated insulin resistance and energy metabolism disorder in PCOS mice as indicated by the upregulation of fasting blood glucose levels, fasting insulin, homeostasis model assessment of insulin resistance (HOMA-IR) index, and weight. Studies have shown that exosomes are involved in the development of follicles. For instance, follicular

fluid-derived exosomes have been reported to regulate follicular dysplasia in PCOS by modulating glycolysis in granulosa cells [35]. Our research showed that the ovaries of PCOS mice treated with adipocyte-derived

exosomes had an increased number of CFs and deteriorated CL, indicating that exosomes from adipocytes affect follicle growth and development. In addition, DHEA-induced PCOS mice had increased
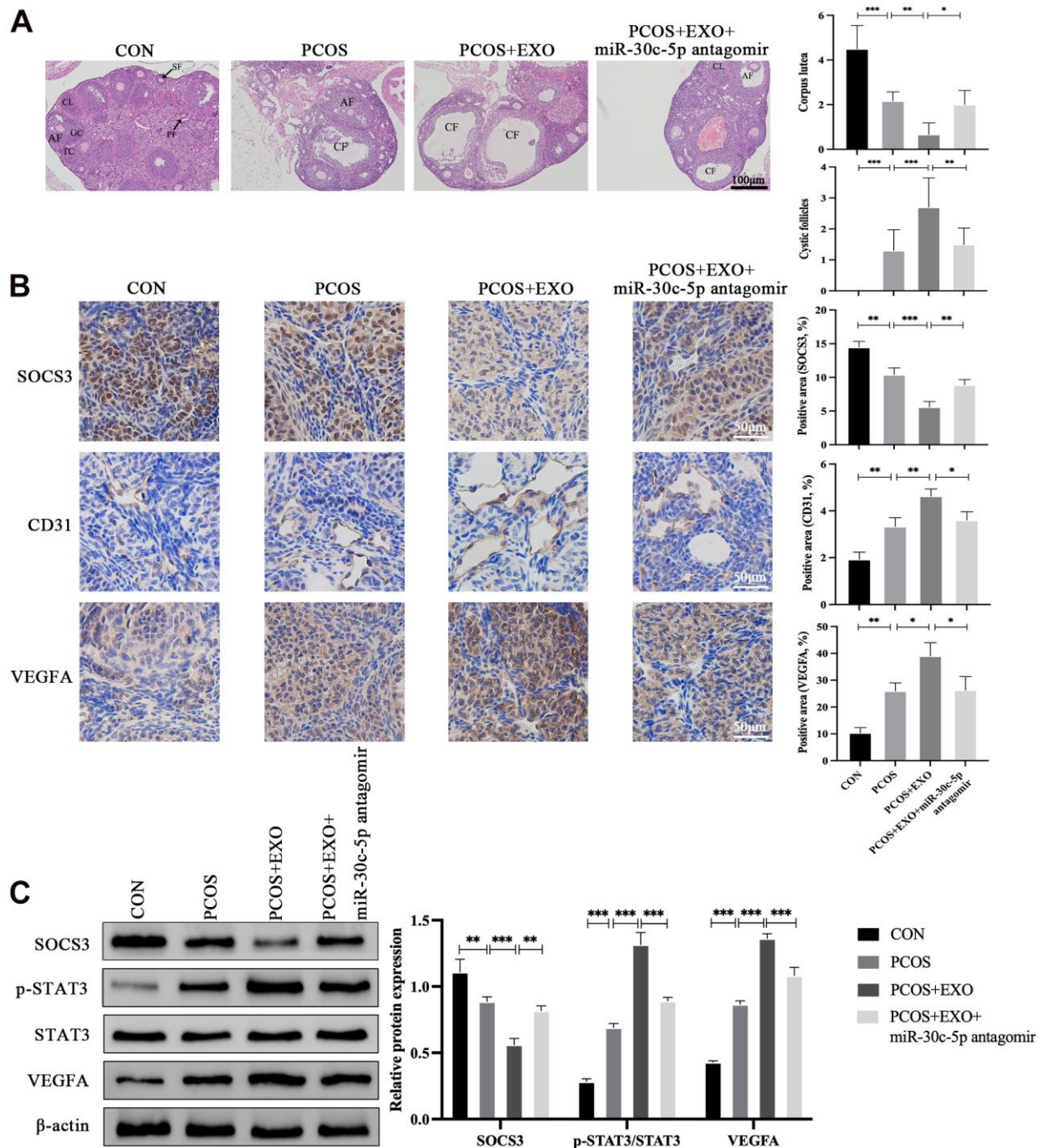

Figure 8. Adipocyte-derived exosomal miR-30c-5p mediates ovarian angiogenesis through the SOCS3/STAT3/VEGFA pathway. (**A**) Visualization of the ovarian morphology in the indicated groups by HE staining. (**B**) Detection of SOCS3, CD31 and VEGFA expression in the ovaries in the indicated groups by IHC staining. (**C**) Western blotting analyses of the SOCS3/STAT3/VEGFA pathway expression in the indicated groups. Primary follicles (PFs), granulosa cells (GCs), theca cells (TCs), secondary follicles (SFs), antral follicles (AFs), corpus luteum (CL), and cystic follicles (CFs). Data are presented as mean ± SD for three independent experiments. *P<0.05, ** P<0.01, ***P<0.001.

serum T and E$_2$ levels and decreased FSH levels, and adipocyte-derived exosomes further exacerbated these changes in sex hormones. However, the exact mechanism remains unknown and needs more research.

As a highly conserved miRNA, miR-30c is considered a multifunctional regulator of cell proliferation, differentiation, and metabolism [36]. A previous study indicated that mesenchymal stem cell-derived exosomes promote angiogenesis by transferring miR-30c [37]. In our research, miR-30c-5p levels were higher in ovaries of PCOS mice. Inhibition of miR-30c-5p alleviated the effects of adipocyte-derived exosomes on the biological behaviour and VEGFA expression in HOMECs as well as endocrine alterations and ovarian angiogenesis in PCOS mice, indicating adipocyte-derived exosomes exert the above effects through miR-30c-5p. However, miR-30c-5p did not significantly affect the estrous cycle of PCOS mice, possibly because there exist other mechanisms regulating estrous cycle.

SOCS is a protein family of eight members (SOCS1–7 and cytokine-induced SH2 protein) that inhibit STAT activation by suppressing the Janus kinase (JAK)/STAT pathway [38]. After cytokines such as interleukin-6 (IL-6) bind to their receptors, receptor-associated JAK proteins are activated via transphosphorylation. JAK activation triggers phosphorylation of tyrosine on the cytoplasmic tail subunit of docking site receptor of the STAT protein. This phosphorylation results in phosphorylation and dimerization of STAT proteins and translocation of dimers to the nucleus, where they integrate with DNA and activate the transcription of response genes such as cyclins, antiapoptotic proteins, VEGF, matrix metalloproteinases and immunosuppressive proteins [39–41]. As a negative regulator of angiogenesis, SOCS3 contains a short N-terminal kinase inhibitory region like that of JAK substrates, which enables them to inhibit signalling by directly inhibiting the catalytic activity of JAKs [42, 43] (Figure 9). Previous studies have revealed that SOCS3 knockdown results in greater phosphorylation and activation of STAT3, thereby upregulating VEGFA and promoting angiogenesis [29, 30]. In addition, a study has reported downregulation of SOCS3 and upregulation of p-STAT3 in ovaries of PCOS rats, which is consistent
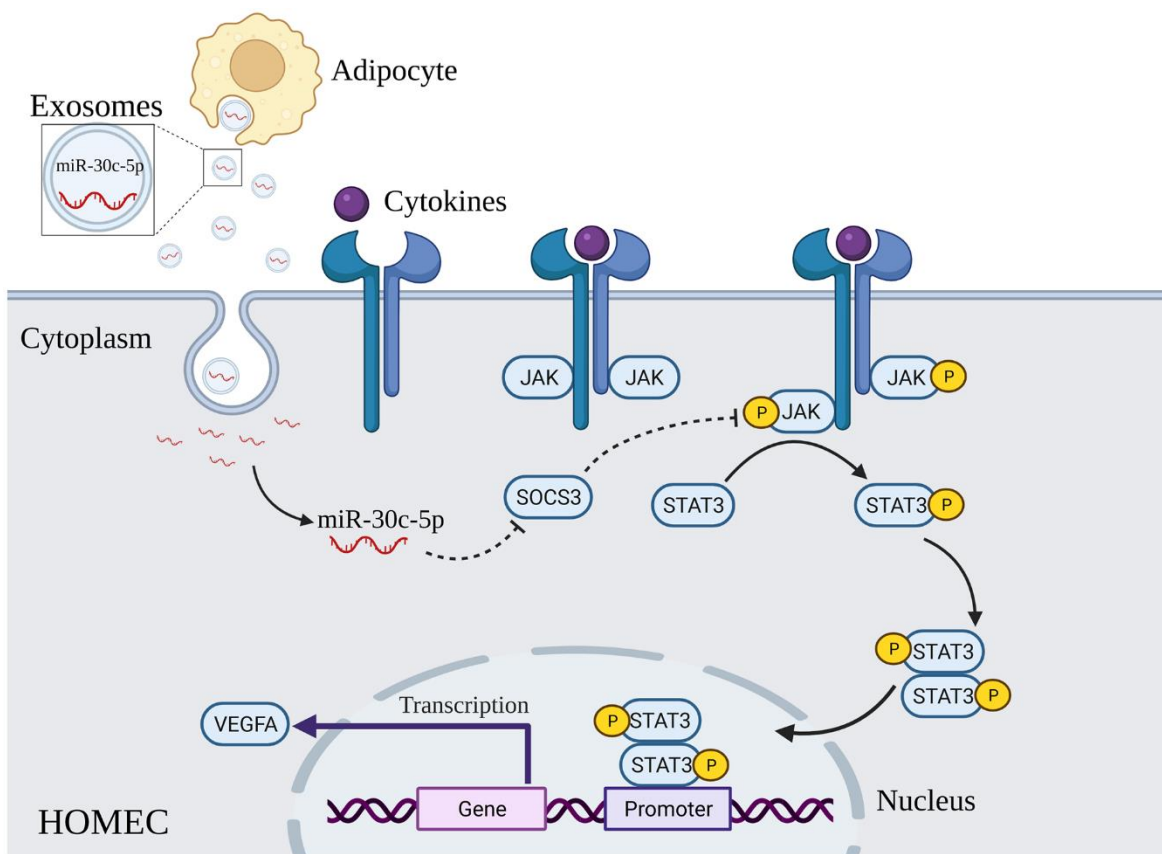

Figure 9. Schematic illustration of adipocyte-derived exosomal miR-30c-5p activating the STAT3/VEGFA pathway by targeting SOCS3 in HOMECs. Exosomes derived from adipocytes promote the activation of the STAT3/VEGFA pathway in HOMECs by transporting miR-30c-5p to directly inhibit SOCS3 expression at the post-transcriptional level.

with our findings in PCOS mice [44]. Besides, our study also showed that adipocyte-derived exosomal miR-30c-5p activated the STAT3/VEGFA pathway *in vivo* and *in vitro* by targeting SOCS3. Altogether, we believe adipocyte-derived exosomal miR-30c-5p regulates ovarian angiogenesis in PCOS via the SOCS3/STAT3/VEGFA pathway.

However, this study has some limitations. First, cells used in this study were obtained from cell lines, which cannot completely simulate the state of specific cells in patients with PCOS. Second, we did not examine the effects of adipocyte-derived exosomes on healthy mice. Third, there might be other exosomal contents mediating the biological effects of adipocyte-derived exosomes. Nevertheless, to the best of our knowledge, this study is the first to examine the role of adipocyte-derived exosomes in the development of PCOS. Hence, this study is of great significance and provides novel insights into the role of exosomes in PCOS. In the future, we plan to conduct more studies to overcome the abovementioned limitations and discover more detailed mechanisms of adipocyte-derived exosomes participating in the development of PCOS.

In conclusion, adipocyte-derived exosomal miR-30c-5p promotes angiogenesis and activates the STAT3/VEGFA pathway by targeting SOCS3, thus contributing to abnormal ovarian angiogenesis in PCOS. This intercellular communication regulated by exosomes may provide new ideas for developing individualized diagnostic and therapeutic strategies for PCOS.

MATERIALS AND METHODS

Cell line and culture

Preadipocyte 3T3-L1 cells were obtained from the American Type Culture Collection (ATCC) and cultured in Dulbecco's Modified Eagle's Medium (DMEM, Gibco) containing 10% fetal bovine serum (FBS, 10099141c, Gibco) and 1% penicillin–streptomycin (Biosharp). HOMECs were obtained from Zhongqiaoxinzhou Biotechnology Co. and cultured in Endothelial Cell Medium (1001, Zhongqiaoxinzhou Biotechnology Co.) containing 5% fetal bovine serum, 1% endothelial cell growth supplement and 1% penicillin–streptomycin. All cells were cultivated in a 5% CO_2 incubator at 37° C.

Adipogenic differentiation

For adipogenic differentiation, 2 days after confluence (day 0), 3T3-L1 cells were incubated in DMEM containing 10% FBS, 1 μM dexamethasone (D4902, Sigma-Aldrich), 0.5 mM 1-methyl-3-isobutylxanthine

(I7018, Sigma-Aldrich) and 10 μg/mL insulin (I5500, Sigma-Aldrich) for 4 days. On day 4, the medium was replaced with DMEM containing 10% FBS and 10 μg/mL insulin for 2 days. Afterwards, the cells were maintained in DMEM containing 10% FBS until day 12. All medium was changed every 2 days.

On day 12, differentiated 3T3-L1 cells were washed twice with PBS and fixed in 4% paraformaldehyde for 20 min. Subsequently, the cells were stained with 60% oil red O (3:2, oil red O saturated solution in isopropanol:distilled water) for 30 min at room temperature. The stained cells were photographed using an inverted microscope (IX51, Olympus).

Exosome isolation and identification

On day 12 of adipogenic differentiation, the medium was replaced with DMEM containing 10% exosome-depleted FBS (EXO-FBS-50A-1, System Biosciences), where differentiated 3T3-L1 cells were cultured for 48 h. The supernatant was collected and centrifuged at 1,000 ×*g* for 10 min, 3,000 ×*g* for 30 min and 10,000×*g* for 20 min at 4° C to separate cell components and fragments. The supernatant from the final centrifugation was ultracentrifuged at 100,000×*g* for 1 h at 4° C, and then the exosome pellet was resuspended in PBS and centrifuged at 100,000×*g* for another 1 h at 4° C [45]. Thereafter, exosomes were resuspended in PBS for further use.

For exosome identification, TEM (HT77000, Hitachi) was applied to determine the morphological features of exosomes. In addition, western blotting was used for detecting the specific exosome markers CD9, CD63 and FABP4. Meanwhile, NTA was used for measuring the particle size and concentration of exosomes using the ZetaView system (PMX 110, Particle Metrix).

In vitro exosome uptake assay

Exosomes were labelled with the red fluorescence dye PKH26 (MX4021, MKbio) according to the manufacturer's instructions. HOMECs were cultured with PKH26-labelled exosomes for 6 h in shade and fixed in 4% paraformaldehyde for 30 min. The cytoskeletons of cells were stained with fluorescein isothiocyanate (FITC)-labelled phalloidin (40735ES75, YEASEN), and nuclei were stained with 4',6-diamidino-2-phenylindole (DAPI, AS1075, ASPEN). The images were captured using an inverted fluorescent microscope (IX51, Olympus).

Cell counting kit-8 assay

Cells in the logarithmic growth phase were suspended in serum-free medium, seeded in 96-well plates at a density of 1×10^3 cells/well and cultured overnight. The serum-

free medium was replaced with a medium containing 10% exosome-depleted FBS on the following day, and the cells were incubated for 0, 12, 24, 48 and 96 h. Subsequently, the CCK-8 (C0038, Beyotime) reagent was added, and then the cells were placed in an incubator at 37° C for 2 h. The optical density value was recorded on a microplate reader (Ensight, Perkin Elmer) at a wavelength of 450 nm.

Transwell assay

Transwell assay was performed in transwell chambers with a pore size of 8.0 μm (3422, Corning). Briefly, 2×10^4 HOMECs suspended in 200 μL of serum-free medium were added to the upper chamber, and 600 μL of medium containing 10% exosome-depleted FBS was added to the lower chamber. The cells were incubated at 37° C for 24 h. Subsequently, the medium was removed, and 4% paraformaldehyde was used to fix the cells for 30 min. The cells were stained with 0.1% (w/v) crystal violet for 10 min, and the migrated cells were visualized and imaged using an optical microscope.

Wound healing assay

For wound healing assay, 2×10^5 cells/well were seeded in a 6-well plate and grown to confluence. The monolayer was scratched using a pipette tip, and then the detached cells were removed using serum-free medium. Thereafter, the cells were cultured in medium supplemented with 10% exosome-depleted FBS at 37° C for 24 h and photographed at 0 h and 24 h after the scratch. Wound closure was calculated as follows: wound recovery area (%) = $(A_0 - A_1)/A_0 \times 100$, where A_0 represents the initial wound area, and A_1 represents the wound area at the time of measurement.

Tube formation assay

Tube formation assay was performed for determining the capillary-like structure formation capacity of HOMECs. Thawed Matrigel matrix (354248, Corning) was added to a 96-well plate and incubated at 37° C for 1 h. Thereafter, the cells were seeded in a 96-well plate at a density of 2×10^4 cells/well and incubated at 37° C. After 6 h, capillary-like structure formation was observed using an inverted microscope.

Coculture

A transwell system (3412, Corning) was used for coculture of differentiated adipocytes and HOMECs. In the coculture experiments, differentiated adipocytes were cultured in the upper chambers, and GW4869 (MedChemExpress) was added to block the secretion of exosomes from adipocytes. Then HOMECs were seeded in the bottom chambers and cocultured with adipocytes for 48 h. qRT-PCR was used to detect the levels of miR-30c-5p in HOMECs.

Cell transfection

miR-30c-5p mimics, inhibitors and the corresponding NCs were obtained from RiboBio Co.. Cells were cultured in a 6-well plate until 70% confluence was achieved. The transfection reagent was prepared by adding the miRNA mimics, inhibitors, or NCs and Lipofectamine 2000 (Lipo 2000, Invitrogen) to serum-free medium, which was incubated at room temperature for 15 min. Subsequently, the reagent was added to each group of cells and incubated at 37° C for 24 h. Transfected cells were treated with fresh medium for 4–6 h before further analyses [46].

The SOCS3 plasmid (*pEnCMV-SOCS3[human]-6×His-SV40-Neo*) and control vector (*pEnCMV-MCS-6×His-SV40-Neo*) were obtained from MiaoLing Biotechnology Co.. The transfection method mentioned above was also applied for plasmid transfection and co-transfection of miR-30c-5p mimics with the SOCS3 plasmid.

Bioinformatic analysis

The target genes of miR-30c-5p were jointly predicted using TargetScan (http://www.targetscan.org/vert_71/), Starbase (https://starbase.sysu.Edu.cn/index.php) and miRDB (http://mirdb.org/). Evenn (http://www.ehbio.com/test/venn/#/) was used to combine the data and determine potential target genes. TargetScan was used to identify the seed sequences and regions of potential base-pairing of the target gene.

Dual luciferase reporter assay

The 3'-UTR of the SOCS3 gene was cloned into a dual luciferase reporter vector (Genepharma), referred to as *pmirGLO-SOCS3-WT*, and a mutant type of the SOCS3 3'-UTR reporter plasmid (*pmirGLO-SOCS3-MUT*) was also generated by altering the seed region. *pmirGLO-SOCS3-WT/MUT* was co-transfected with miR-30c-5p mimics into HOMECs using Lipofectamine 2000 for 48 h. Finally, the dual luciferase reporter gene assay kit (Genepharma) was used to measure the binding activity of miR-30c-5p based on firefly/renilla luciferase activity.

Animals and experimental protocol

Female C57BL/6J mice (N=42, 21 days old) were raised at a controlled temperature between 22 and 24° C,

with free access to food and water. The PCOS model group (N=32) was subcutaneously injected with dehydroepiandrosterone (DHEA) (6 mg/100 g weight in sesame oil) daily for 21 days to induce PCOS [47]. The control group (CON, N=10) was injected with sesame oil. The establishment of PCOS models was determined by weight, estrous cycle, and ovarian morphology. DHEA-induced PCOS mice were divided into the following three groups: PCOS control group(N=10), PCOS+EXO group (N=12) and PCOS+EXO+miR-30c-5p antagomir group (N=10). Exosomes (30 μg in 200 μL PBS) and miR-30c-5p antagomir (10 mg/kg) were injected into PCOS mice twice a week via the tail vein for 2 weeks [48, 49]. During the treatment period, the mice were weighed weekly, and the estrous cycle was assessed daily via vaginal smears from the 10th day of the first DHEA injection until the end of the experiment. At the end of the treatment period, fasting blood glucose levels were measured via the tail vein after 12 h of fasting using a blood glucose meter (Sinocare). Thereafter, the blood of all mice was collected from the heart using a 1 mL syringe under isoflurane anaesthesia. Serum samples were collected via centrifugation and stored at −80° C for further analyses, and the ovaries were removed for conducting additional experiments. All protocols and experiments were approved by the Animal Care and Use Committee of Renmin Hospital of Wuhan University.

In vivo exosome uptake assay

For verification of adipocyte-derived exosomes being taken up by ovaries, PKH26-labeled exosomes were injected into PCOS mice via tail vein. After 24h, the mice were sacrificed, and the ovaries were collected for further IF analyses. For IF staining, the harvested sections were incubated with the primary antibody CD31 (sc-376764, Santa Cruz, 1:100). Subsequently, the sections were incubated with Alexa Fluor 488-conjugated secondary antibody and stained with DAPI for visualization. The fluorescence expression of CD31, DAPI and PKH26-labelled exosomes was determined using a fluorescence microscope.

Ovarian morphology

The ovaries were incubated with paraformaldehyde, dehydrated with ethanol of different concentrations, and embedded with paraffin wax. The maximum cross-section of the ovaries was cut and stained with haematoxylin and eosin (HE). The follicles were classified as primary follicles (PFs) with one layer of cubical granulosa cells (GCs), secondary follicles (SFs) with two or more layers of GCs and antral follicles (AFs) based on the presence or absence of an antrum and CL. CFs contain an attenuated GC layer and

thickened theca interna cell layer with a large antrum or a large fluid-filled structure [50].

Elisa

The levels of VEGFA, E_2, T, FSH and insulin in the serum were measured using sandwich ELISA kits (Servicebio, Wuhan, China) according to the manufacturer's instructions. Each sample was measured in duplicate.

Immunohistochemical

For IHC staining, tissue sections were deparaffinized and rehydrated with xylene and ethanol. The endogenous peroxidase activity was blocked using H_2O_2 in PBS, and non-specific binding was blocked using 5% BSA. Subsequently, the sections were incubated with biotinylated IgG (ASPEN), followed by incubation with the primary antibodies CD31 (#92841, CST, 1:200), VEGFA (ab52917, Abcam, 1:100) and SOCS3 (ab280884, Abcam, 1:1000). Finally, the sections were visualized using the chromogenic substrate diaminobenzidine, and an optical microscope (BX51, Olympus) was used to capture images of the stained sections.

qRT-PCR analysis

Total RNA in cells and the ovaries was isolated using the TRIzol reagent (Life Technology), and cDNA for miRNAs was synthesised using the miRNA First Strand cDNA Synthesis kit (Sangon) according to the manufacturer's instructions. qRT-PCR was performed using a miRNA qPCR Kit (Sangon) with the forward primer and the universal reverse primer of miR-30c-5p (Sangon). Gene expression was evaluated using the $2^{-\Delta\Delta CT}$ method [51], and U6 was used to normalize the relative expression of miR-30c-5p. The primer sequences used are as follows: miR-30c-5p forward primer, *5´-GCTGCGTGTAAACATCCTACACT-3´*; reverse primer, *5´-AGTGCAGGGTCCGAGGTATT-3´* and U6 forward primer, *5´- CTCGCTTCGGCAGCACA-3´*; reverse primer, *5´- AACGCTTCACGAATTTGCGT -3´*.

Western blotting analysis

Cell and tissue proteins were extracted using Radio Immunoprecipitation Assay (RIPA) buffer (ASPEN). The concentrations of proteins were detected by a BCA Protein Assay Kit (P0010, Beyotime) according to the manufactures' instructions. Protein extracts were separated via sodium dodecyl sulfate–polyacrylamide gel electrophoresis (SDS-PAGE) and transferred onto polyvinylidene fluoride (PVDF) membranes. The membranes were blocked with 5% milk in Tris-buffered

saline containing 0.1% Tween-20 for 1 h at room temperature. Subsequently, the membranes were incubated with primary antibodies at 4° C overnight, followed by incubation with horseradish peroxidase (HRP)-labelled secondary antibodies at 37° C for 1 h. The antibodies included rabbit anti-CD9 (ab92726, Abcam, 1:1000), mouse anti-CD63 (sc-5275, Santa Cruz, 1:500), rabbit anti-FABP4 (ab92501, Abcam, 1:2000), rabbit anti-Ki67 (ab16667, Abcam, 1:500), rabbit anti-PCNA (#13110, CST, 1:1000), rabbit anti-Vimentin (#5741, CST, 1:500), mouse anti-E-cadherin (#14472, CST, 1:500), rabbit anti-VEGFA (ab46154, Abcam, 1:1000), rabbit anti-SOCS3 (ab280884, Abcam, 1:1000), rabbit anti-STAT3 (sc-8019, Santa Cruz, 1:500), rabbit anti-p-STAT3 (sc-8059, Santa Cruz, 1:500), HRP-labelled goat anti-rabbit (ASPEN) and HRP-labelled goat anti-mouse (ASPEN) antibodies. Rabbit anti-GAPDH (ab37168, Abcam, 1:10000) and rabbit anti-β-actin (ab8227, Abcam, 1:5000) were used as the internal reference. The immunoreactive bands were visualized on an ECL-Plus western blotting detection system (Thermo Fisher Scientific). The ratio of the grey value of the target band to the internal reference band was used to assess the relative expression of the protein.

Statistical analysis

All data were analyzed using the SPSS Statistics (version 26.0) (IBM) and Prism 9 (GraphPad) software. Data were expressed as mean ± standard deviation (SD) of at least three independent experiments. Student's t-test was used to compare data between two groups, and one-way ANOVA followed by Tukey's multiple comparison test was used to compare data among multiple groups. Statistical significance was established at $*P < 0.05$ versus the indicated group.

Data availability

All data generated or analyzed during this study are included in this published article.

Abbreviations

AFs: antral follicles; AT: adipose tissue; ATCC: American type culture collection; CCK-8: cell counting kit-8; CFs: cystic follicles; CL: corpus luteum; DAPI: 4':6-diamidino-2-phenylindole; DHEA: dehydroepiandrosterone; DMEM: Dulbecco's modified eagle's medium; ECs: endothelial cells; EVs: extracellular vesicles; FBS: fetal bovine serum; FITC: fluorescein isothiocyanate; FSH: follicle-stimulating hormone; GCs: granulosa cells; HE: hematoxylin and eosin; HOMA-IR: homeostasis model assessment of insulin resistance; HOMECs: human ovarian microvascular endothelial cells; HRP: horseradish peroxidase; HUVECs: human umbilical vein endothelial cells; IF: immunofluorescence; IHC: immunohistochemical; IL-6: interleukin-6; JAK: Janus kinase; miRNAs: microRNAs; ncRNAs: noncoding RNAs; NTA: nanoparticle tracking analysis; PBS: phosphate-buffered saline; PCNA: proliferating cell nuclear antigen; PCOS: polycystic ovary syndrome; PFs: primary follicles; PVDF: polyvinylidene fluoride; RIPA: radio immunoprecipitation assay; SD: standard deviation; SDS-PAGE: sodium dodecyl sulfate–polyacrylamide gel electrophoresis; SFs: secondary follicles; SNHG9: small nucleolar RNA host gene 9; SOCS3: suppressor of cytokine signaling 3; STAT3: signal transducer and activator of transcription 3; T: testosterone; TEM: transmission electron microscopy; TRADD: TNF receptor-associated death domain; UTR: untranslated region; VEGF: vascular endothelial growth factor; VEGFA: vascular endothelial growth factor A.

AUTHOR CONTRIBUTIONS

JH and FYL designed the study. JH and FYL performed the experiments and drafted the manuscript. JH, FYL, YCY and YJS participated in data analysis. JH, FYL, ZNX and WMX were involved in the discussion and interpretation of results. ZNX and WMX organized the whole project. All authors have read and approved the final manuscript.

CONFLICTS OF INTEREST

The authors declare that they have no conflicts of interest.

Ethical Statement and Consent

All animal protocols were approved (approval no. WDRM-20210612) by the Animal Care and Use Committee of Renmin Hospital of Wuhan University and conducted in accordance with the National Institutes of Health Guide for the Care and Use of Laboratory Animals.

REFERENCES

1. Escobar-Morreale HF. Polycystic ovary syndrome: definition, aetiology, diagnosis and treatment. Nat Rev Endocrinol. 2018; 14:270–84.
https://doi.org/10.1038/nrendo.2018.24
PMID:29569621

2. Rotterdam ESHRE/ASRM-Sponsored PCOS consensus workshop group. Revised 2003 consensus on diagnostic criteria and long-term health risks related to polycystic ovary syndrome (PCOS). Hum Reprod. 2004; 19:41–7.
https://doi.org/10.1093/humrep/deh098
PMID:14688154

3. Stapor P, Wang X, Goveia J, Moens S, Carmeliet P. Angiogenesis revisited - role and therapeutic potential of targeting endothelial metabolism. J Cell Sci. 2014; 127:4331–41.
https://doi.org/10.1242/jcs.153908 PMID:25179598

4. Duncan WC, Nio-Kobayashi J. Targeting angiogenesis in the pathological ovary. Reprod Fertil Dev. 2013; 25:362–71.
https://doi.org/10.1071/RD12112
PMID:22951108

5. Dwivedi AN, Ganesh V, Shukla RC, Jain M, Kumar I. Colour Doppler evaluation of uterine and ovarian blood flow in patients of polycystic ovarian disease and post-treatment changes. Clin Radiol. 2020; 75:772–9.
https://doi.org/10.1016/j.crad.2020.05.023
PMID:32660710

6. Alcázar JL, Kudla MJ. Ovarian stromal vessels assessed by spatiotemporal image correlation-high definition flow in women with polycystic ovary syndrome: a case-control study. Ultrasound Obstet Gynecol. 2012; 40:470–5.
https://doi.org/10.1002/uog.11187
PMID:22605534

7. Di Pietro M, Pascuali N, Parborell F, Abramovich D. Ovarian angiogenesis in polycystic ovary syndrome. Reproduction. 2018; 155:R199–209.
https://doi.org/10.1530/REP-17-0597
PMID:29386378

8. Kamat BR, Brown LF, Manseau EJ, Senger DR, Dvorak HF. Expression of vascular permeability factor/vascular endothelial growth factor by human granulosa and theca lutein cells. Role in corpus luteum development. Am J Pathol. 1995; 146:157–65.
PMID:7531945

9. Dambala K, Vavilis D, Bili E, Goulis DG, Tarlatzis BC. Serum visfatin, vascular endothelial growth factor and matrix metalloproteinase-9 in women with polycystic ovary syndrome. Gynecol Endocrinol. 2017; 33:529–33.
https://doi.org/10.1080/09513590.2017.1296425
PMID:28300464

10. Artini PG, Monti M, Matteucci C, Valentino V, Cristello F, Genazzani AR. Vascular endothelial growth factor and basic fibroblast growth factor in polycystic ovary syndrome during controlled ovarian hyperstimulation. Gynecol Endocrinol. 2006; 22:465–70.
https://doi.org/10.1080/09513590600906607
PMID:17012110

11. Elci E, Kaya C, Cim N, Yildizhan R, Elci GG. Evaluation of cardiac risk marker levels in obese and non-obese patients with polycystic ovaries. Gynecol Endocrinol. 2017; 33:43–7.
https://doi.org/10.1080/09513590.2016.1203893
PMID:27425379

12. Agrawal R, Conway G, Sladkevicius P, Tan SL, Engmann L, Payne N, Bekir J, Campbell S, Jacobs H. Serum vascular endothelial growth factor and Doppler blood flow velocities in *in vitro* fertilization: relevance to ovarian hyperstimulation syndrome and polycystic ovaries. Fertil Steril. 1998; 70:651–8.
https://doi.org/10.1016/s0015-0282(98)00249-0
PMID:9797093

13. Rashid R, Mir SA, Kareem O, Ali T, Ara R, Malik A, Amin F, Bader GN. Polycystic ovarian syndrome-current pharmacotherapy and clinical implications. Taiwan J Obstet Gynecol. 2022; 61:40–50.
https://doi.org/10.1016/j.tjog.2021.11.009
PMID:35181044

14. de Medeiros SF, Rodgers RJ, Norman RJ. Adipocyte and steroidogenic cell cross-talk in polycystic ovary syndrome. Hum Reprod Update. 2021; 27:771–96.
https://doi.org/10.1093/humupd/dmab004
PMID:33764457

15. Pegtel DM, Gould SJ. Exosomes. Annu Rev Biochem. 2019; 88:487–514.
https://doi.org/10.1146/annurev-biochem-013118-111902 PMID:31220978

16. Lanthier N, Leclercq IA. Adipose tissues as endocrine target organs. Best Pract Res Clin Gastroenterol. 2014; 28:545–58.
https://doi.org/10.1016/j.bpg.2014.07.002
PMID:25194174

17. Yu Y, Du H, Wei S, Feng L, Li J, Yao F, Zhang M, Hatch GM, Chen L. Adipocyte-Derived Exosomal MiR-27a Induces Insulin Resistance in Skeletal Muscle Through Repression of PPARγ. Theranostics. 2018; 8:2171–88.
https://doi.org/10.7150/thno.22565 PMID:29721071

18. Sano S, Izumi Y, Yamaguchi T, Yamazaki T, Tanaka M, Shiota M, Osada-Oka M, Nakamura Y, Wei M, Wanibuchi H, Iwao H, Yoshiyama M. Lipid synthesis is promoted by hypoxic adipocyte-derived exosomes in

3T3-L1 cells. Biochem Biophys Res Commun. 2014; 445:327–33.
https://doi.org/10.1016/j.bbrc.2014.01.183
PMID:24513287

19. Song Y, Li H, Ren X, Li H, Feng C. SNHG9, delivered by adipocyte-derived exosomes, alleviates inflammation and apoptosis of endothelial cells through suppressing TRADD expression. Eur J Pharmacol. 2020; 872:172977.
https://doi.org/10.1016/j.ejphar.2020.172977
PMID:32007500

20. Thomou T, Mori MA, Dreyfuss JM, Konishi M, Sakaguchi M, Wolfrum C, Rao TN, Winnay JN, Garcia-Martin R, Grinspoon SK, Gorden P, Kahn CR. Adipose-derived circulating miRNAs regulate gene expression in other tissues. Nature. 2017; 542:450–5.
https://doi.org/10.1038/nature21365
PMID:28199304

21. Irani S, Hussain MM. Role of microRNA-30c in lipid metabolism, adipogenesis, cardiac remodeling and cancer. Curr Opin Lipidol. 2015; 26:139–46.
https://doi.org/10.1097/MOL.0000000000000162
PMID:25692340

22. Moghiman T, Barghchi B, Esmaeili SA, Shabestari MM, Tabaee SS, Momtazi-Borojeni AA. Therapeutic angiogenesis with exosomal microRNAs: an effectual approach for the treatment of myocardial ischemia. Heart Fail Rev. 2021; 26:205–13.
https://doi.org/10.1007/s10741-020-10001-9
PMID:32632768

23. Karbiener M, Neuhold C, Opriessnig P, Prokesch A, Bogner-Strauss JG, Scheideler M. MicroRNA-30c promotes human adipocyte differentiation and co-represses PAI-1 and ALK2. RNA Biol. 2011.
https://doi.org/10.4161/rna.8.5.16153
PMID:21878751

24. Bridge G, Monteiro R, Henderson S, Emuss V, Lagos D, Georgopoulou D, Patient R, Boshoff C. The microRNA-30 family targets DLL4 to modulate endothelial cell behavior during angiogenesis. Blood. 2012; 120:5063–72.
https://doi.org/10.1182/blood-2012-04-423004
PMID:23086751

25. Long W, Zhao C, Ji C, Ding H, Cui Y, Guo X, Shen R, Liu J. Characterization of serum microRNAs profile of PCOS and identification of novel non-invasive biomarkers. Cell Physiol Biochem. 2014; 33:1304–15.
https://doi.org/10.1159/000358698
PMID:24802714

26. Ferrante SC, Nadler EP, Pillai DK, Hubal MJ, Wang Z, Wang JM, Gordish-Dressman H, Koeck E, Sevilla S, Wiles AA, Freishtat RJ. Adipocyte-derived exosomal miRNAs: a novel mechanism for obesity-related disease. Pediatr Res. 2015; 77:447–54.
https://doi.org/10.1038/pr.2014.202
PMID:25518011

27. Wang F, Chen FF, Shang YY, Li Y, Wang ZH, Han L, Li YH, Zhang L, Ti Y, Zhang W, Zhong M. Insulin resistance adipocyte-derived exosomes aggravate atherosclerosis by increasing vasa vasorum angiogenesis in diabetic ApoE-/- mice. Int J Cardiol. 2018; 265:181–7.
https://doi.org/10.1016/j.ijcard.2018.04.028
PMID:29685689

28. Gao XR, Ge J, Li WY, Zhou WC, Xu L, Geng DQ. miR-34a carried by adipocyte exosomes inhibits the polarization of M1 macrophages in mouse osteolysis model. J Biomed Mater Res A. 2021; 109:994–1003.
https://doi.org/10.1002/jbm.a.37088 PMID:32803914

29. Sun Y, Ju M, Lin Z, Fredrick TW, Evans LP, Tian KT, Saba NJ, Morss PC, Pu WT, Chen J, Stahl A, Joyal JS, Smith LE. SOCS3 in retinal neurons and glial cells suppresses VEGF signaling to prevent pathological neovascular growth. Sci Signal. 2015; 8:ra94.
https://doi.org/10.1126/scisignal.aaa8695
PMID:26396267

30. Yan Z, Hong S, Song Y, Bi M. microR-4449 Promotes Colorectal Cancer Cell Proliferation via Regulation of SOCS3 and Activation of STAT3 Signaling. Cancer Manag Res. 2021; 13:3029–39.
https://doi.org/10.2147/CMAR.S266153
PMID:33854373

31. Crewe C, Joffin N, Rutkowski JM, Kim M, Zhang F, Towler DA, Gordillo R, Scherer PE. An Endothelial-to-Adipocyte Extracellular Vesicle Axis Governed by Metabolic State. Cell. 2018; 175:695–708.e13.
https://doi.org/10.1016/j.cell.2018.09.005
PMID:30293865

32. Apte RS, Chen DS, Ferrara N. VEGF in Signaling and Disease: Beyond Discovery and Development. Cell. 2019; 176:1248–64.
https://doi.org/10.1016/j.cell.2019.01.021
PMID:30849371

33. Song M, Han L, Chen FF, Wang D, Wang F, Zhang L, Wang ZH, Zhong M, Tang MX, Zhang W. Adipocyte-Derived Exosomes Carrying Sonic Hedgehog Mediate M1 Macrophage Polarization-Induced Insulin Resistance via Ptch and PI3K Pathways. Cell Physiol Biochem. 2018; 48:1416–32.
https://doi.org/10.1159/000492252 PMID:30064125

34. Gao J, Li X, Wang Y, Cao Y, Yao D, Sun L, Qin L, Qiu H, Zhan X. Adipocyte-derived extracellular vesicles modulate appetite and weight through mTOR signalling in the hypothalamus. Acta Physiol (Oxf). 2020; 228:e13339.
https://doi.org/10.1111/apha.13339
PMID:31278836

35. Cao J, Huo P, Cui K, Wei H, Cao J, Wang J, Liu Q, Lei X, Zhang S. Follicular fluid-derived exosomal miR-143-3p/miR-155-5p regulate follicular dysplasia by modulating glycolysis in granulosa cells in polycystic ovary syndrome. Cell Commun Signal. 2022; 20:61.
https://doi.org/10.1186/s12964-022-00876-6
PMID:35534864

36. Han W, Cui H, Liang J, Su X. Role of MicroRNA-30c in cancer progression. J Cancer. 2020; 11:2593–601.
https://doi.org/10.7150/jca.38449
PMID:32201529

37. Gong M, Yu B, Wang J, Wang Y, Liu M, Paul C, Millard RW, Xiao DS, Ashraf M, Xu M. Mesenchymal stem cells release exosomes that transfer miRNAs to endothelial cells and promote angiogenesis. Oncotarget. 2017; 8:45200–12.
https://doi.org/10.18632/oncotarget.16778
PMID:28423355

38. Carow B, Rottenberg ME. SOCS3, a Major Regulator of Infection and Inflammation. Front Immunol. 2014; 5:58.
https://doi.org/10.3389/fimmu.2014.00058
PMID:24600449

39. Sims NA. The JAK1/STAT3/SOCS3 axis in bone development, physiology, and pathology. Exp Mol Med. 2020; 52:1185–97.
https://doi.org/10.1038/s12276-020-0445-6
PMID:32788655

40. Gao Y, Zhao H, Wang P, Wang J, Zou L. The roles of SOCS3 and STAT3 in bacterial infection and inflammatory diseases. Scand J Immunol. 2018; 88:e12727.
https://doi.org/10.1111/sji.12727 PMID:30341772

41. Zou S, Tong Q, Liu B, Huang W, Tian Y, Fu X. Targeting STAT3 in Cancer Immunotherapy. Mol Cancer. 2020; 19:145.
https://doi.org/10.1186/s12943-020-01258-7
PMID:32972405

42. Rao N, Lee YF, Ge R. Novel endogenous angiogenesis inhibitors and their therapeutic potential. Acta Pharmacol Sin. 2015; 36:1177–90.
https://doi.org/10.1038/aps.2015.73
PMID:26364800

43. Sasaki A, Yasukawa H, Suzuki A, Kamizono S, Syoda T, Kinjyo I, Sasaki M, Johnston JA, Yoshimura A. Cytokine-inducible SH2 protein-3 (CIS3/SOCS3) inhibits Janus tyrosine kinase by binding through the N-terminal kinase inhibitory region as well as SH2 domain. Genes Cells. 1999; 4:339–51.
https://doi.org/10.1046/j.1365-2443.1999.00263.x
PMID:10421843

44. Zhou Y, Lv L, Liu Q, Song J. Total flavonoids extracted from Nervilia Fordii function in polycystic ovary syndrome through IL-6 mediated JAK2/STAT3 signaling pathway. Biosci Rep. 2019; 39:BSR20181380.
https://doi.org/10.1042/BSR20181380
PMID:30463907

45. Wang J, Wu Y, Guo J, Fei X, Yu L, Ma S. Adipocyte-derived exosomes promote lung cancer metastasis by increasing MMP9 activity via transferring MMP3 to lung cancer cells. Oncotarget. 2017; 8:81880–91.
https://doi.org/10.18632/oncotarget.18737
PMID:29137230

46. Lin FY, Han ST, Yu WM, Rao T, Ruan Y, Yuan R, Li HY, Ning JZ, Xia YQ, Xie JN, Qi YC, Zhou XJ, Cheng F. microRNA-486-5p is implicated in the cisplatin-induced apoptosis and acute inflammation response of renal tubular epithelial cells by targeting HAT1. J Biochem Mol Toxicol. 2022; 36:e23039.
https://doi.org/10.1002/jbt.23039 PMID:35279909

47. Xie Q, Xiong X, Xiao N, He K, Chen M, Peng J, Su X, Mei H, Dai Y, Wei D, Lin G, Cheng L. Mesenchymal Stem Cells Alleviate DHEA-Induced Polycystic Ovary Syndrome (PCOS) by Inhibiting Inflammation in Mice. Stem Cells Int. 2019; 2019:9782373.
https://doi.org/10.1155/2019/9782373
PMID:31611920

48. Deng ZB, Poliakov A, Hardy RW, Clements R, Liu C, Liu Y, Wang J, Xiang X, Zhang S, Zhuang X, Shah SV, Sun D, Michalek S, et al. Adipose tissue exosome-like vesicles mediate activation of macrophage-induced insulin resistance. Diabetes. 2009; 58:2498–505.
https://doi.org/10.2337/db09-0216
PMID:19675137

49. Wang X, Guo B, Li Q, Peng J, Yang Z, Wang A, Li D, Hou Z, Lv K, Kan G, Cao H, Wu H, Song J, et al. miR-214 targets ATF4 to inhibit bone formation. Nat Med. 2013; 19:93–100.
https://doi.org/10.1038/nm.3026
PMID:23223004

50. Mao Z, Yang L, Lu X, Tan A, Wang Y, Ding F, Xiao L, Qi X, Yu Y. C1QTNF3 in the murine ovary and its function in folliculogenesis. Reproduction. 2018; 155:333–46.
https://doi.org/10.1530/REP-17-0783
PMID:29438034

51. Schmittgen TD, Livak KJ. Analyzing real-time PCR data by the comparative C(T) method. Nat Protoc. 2008; 3:1101–8.
https://doi.org/10.1038/nprot.2008.73
PMID:18546601

SUPPLEMENTARY MATERIALS

Supplementary Figure
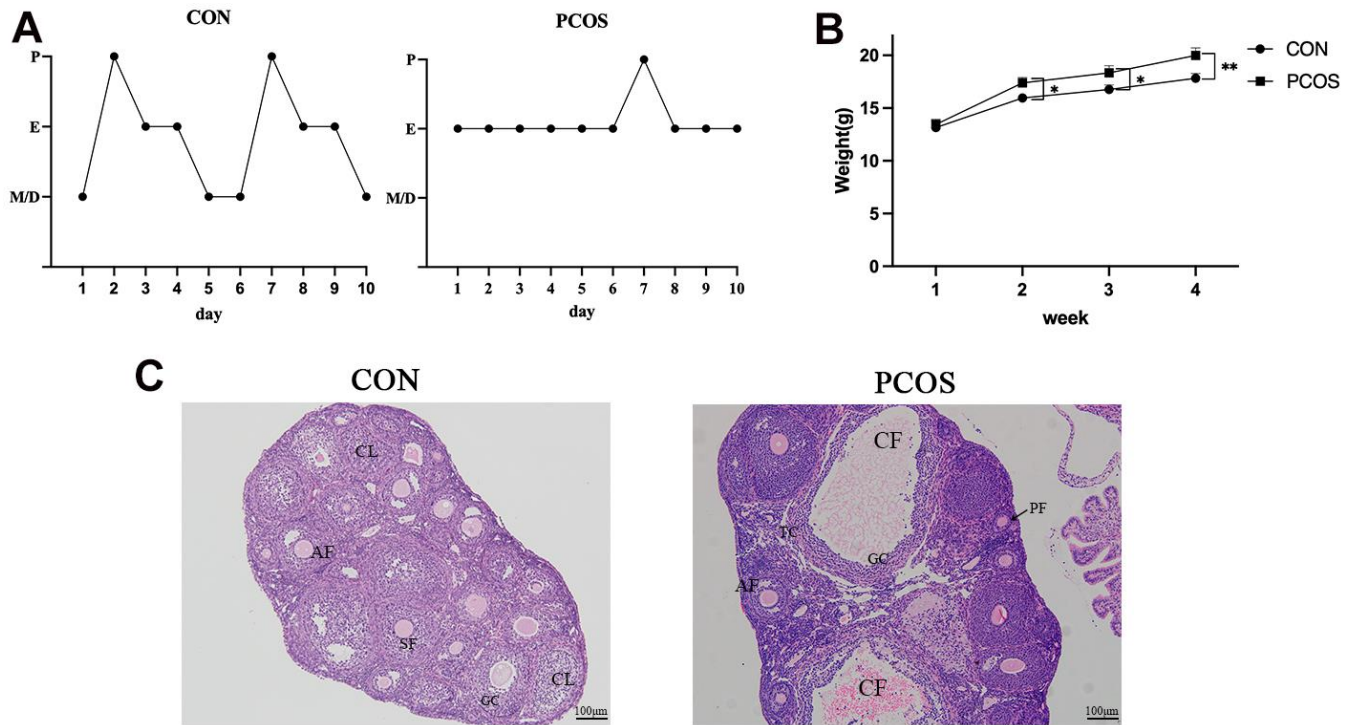
Supplementary Figure 1. The establishment of DHEA-induced PCOS models. (**A**) Estrous cycle analyses of mice in each group via vaginal smears. (**B**) Weight change in each group. (**C**) Representative images of HE staining of morphological features of the ovaries in each group. Proestrus (P), estrus (E), metestrus (M) and diestrus (D). Primary follicles (PFs), granulosa cells (GCs), theca cells (TCs), secondary follicles (SFs), antral follicles (AFs), corpus luteum (CL), and cystic follicles (CFs). *P<0.05, ** P<0.01.